Interlaced layer thicknesses within single laser powder bed fusion geometries

Adam Clare[1*] (2), Alex Gullane[1], Christopher Hyde[1], James W. Murray[1], Simon Sankare[2], Wessel W. Wits[3] (2)

[1]Faculty of Engineering, University of Nottingham, Nottingham, UK
[2]Oerlikon AM GmbH, Feldkirchen, Germany
[3]Faculty of Engineering Technology, University of Twente, Enschede, The Netherlands

The geometrical design freedoms associated with additive manufacturing techniques are currently well exploited and finding commercial application. The capability of layer-based processes to allow modification of composition and microstructure in process to achieve functional grading is currently a growing topic. In this work, a method is demonstrated for varying layer thickness within single components that allows part sections to be interlaced for the purpose of locally manipulating material and structural properties. Demonstrator geometries are explored here which exhibit the interfaces within specimens constituted of both 30μm and 150μm. Accordingly, a new design freedom for laser powder bed fusion is created.

Additive Manufacturing, Selective laser melting (SLM), Tensile strength

1. Introduction

Materials creation and adaptation for Laser Powder Bed Fusion (LPBF) is a fertile research area as the *pallet* of Additive Manufacturing (AM) appropriate materials is broadened. Bourell et al. provided a comprehensive review of this topic and emergent trends [1]. It is clear from this review that focus is being given to development of materials specifically for AM processes. Beyond new materials development, research has also begun to explore adapting process parameters to realise localised material properties while utilising a single material feedstock.

Since LPBF relies upon layers generated from a slicing algorithm and both material and energy delivery are restricted to these domains. Scan strategies have been explored by Catchpole-Smith et al., in which, vectors by design have been used to manage process thermodynamics [2]. Localised scan parameters are widely deployed. An example being the use of 'skin scanning' which allows a superior surface to be created at the contour of parts. This has been further explored by de Formanoir et al. who proposed a 'hull-bulk' strategy for the enhancement of productivity in LPBF [3]. This work highlights an opportunity to enhance production rates through increasing layer thicknesses in build regions, while relying on thinner layers to give detailed contour definitions. The work makes use of 30 and 90 μm layer thicknesses to increase build rates, but the utility of this approach is not explored completely. For instance, simple 'planar' interfaces may be improved by interlacing regions – the basis of this work. Similarly, Sofinowski et al. showed that tailoring of energy provision on a layer-wise basis can allow graduation in the 'z' direction of powder bed processes [4]. No doubt this is a useful technique for extracting additional localised properties from a single feedstock type. However, knowledge is lacking to apply this at component level.

The intent with adapted process controls is to modulate heat loss and hence thermal history, and therefore control recrystallisation. This has been used to attenuate residual stresses by Bartlett et al. [5] and achieve microstructure by design by Acharya et al. [6]. When modifying processes, full consolidation and near 100% density must be achieved such that microstructure and not topology dictates component characteristics. Dense parts can be achieved within a broad parameter set (layer thickness, energy

density and hatch spacing) and understanding of process windows has been enhanced through calorimetry [7], consolidation behaviour [8] and observation of the process mechanics [9] – Clare et al., Tang et al. and Matthews et al. respectively.

There are two principle benefits to enabling both thicker layers in LPBF and enabling 'interlacing' between these regions i) this may be used to engineer processes which have a higher build rate using lower laser on-time and ii) presents a novel way to achieve control over part failure in terms of crack initiation location and propagation direction. This study focuses on fundamental fusion of disparate layer thickness regions in order to establish a foundation of knowledge in this area. Hence the secondary benefit of controlling part failure is not explored to its potential here, but reserved for a later, independent study.

Figure 1 shows formative findings by the authors when evaluating parameter sets for building with larger layer thicknesses. In theory, Volumetric Energy Density (VED) should remain constant since, by definition, it is energy density per unit volume of a constant material. Nonetheless, Figure 1 shows it was necessary to increase VED as the layer thickness increases. This can be attributed to the growing volume of shrinkage as layers become thicker, giving rise to a larger volume deficit prior to powder spreading and greater absolute energy losses. The difference between true layer thickness and nominal layer thickness grows as illustrated in Figure 1.

Also shown in Figure 1, is the need to reduce scan speeds in order to achieve greater VED for a growing layer thickness. Ideally, processing a layer five times thicker (150 μm compared with 30 μm), one might expect to reduce laser-on time to one-fifth. Nonetheless, the need to make use of slower scan speeds means the relationship between layer thickness and laser-on time is not directly proportional. Despite the additional time necessary to process one layer, significant build time reductions can be achieved by only processing regions of a part every five layers, for example; especially for larger parts requiring layer-lasing times to the order of minutes, as well as those featuring large z-heights and hence a high number of total layers. An ideal instance of the method presented in this study achieves a significant build rate increase with no penalty to part quality, such as surface finish or mechanical performance. In practice, some penalty to part quality must be tolerated, and as such is explored here.
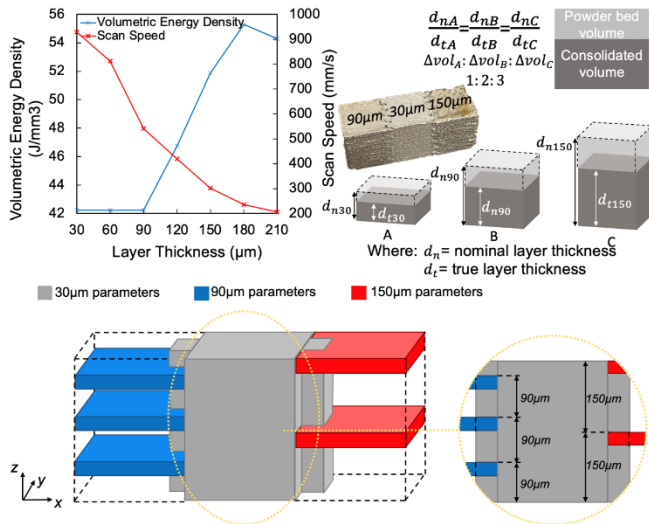
Figure 1. Increasing layer thickness can reduce build time. This typically requires higher energy provision per unit volume. Absolute shrinkage of the consolidated layer becomes more significant at larger layer thicknesses. The lower inset shows a demonstrator arrangement allowing 3-layer thicknesses within a single build.

This study explores the use of interfaces comprised of simple castellated joints (*see* unit cell Figure 1 lower inset) between regions of 30 and 150 μm thickness to demonstrate that interfaces can be created by design. Failure mechanisms in castellated specimens as compared to parent 30 and 150 μm regions are presented and exemplar joint designs are demonstrated for the purpose of accelerating build rates and providing additional means for location specific material properties.

2. Methodology

In this study, a conventional LPBF system (Renishaw AM125) was used to build test specimens and cubes for tensile testing and build evaluation, respectively. Test specimens formed three groups of 30 μm, 150 μm and 30-150 μm castellated (*see* Figure 2) blanks measuring 11 mm in diameter. 'Slicing' was configured to define volumes of differing layer thicknesses within a single entity by defining separate parts which were in contact. Since the Materialise Autofab slicing software was not designed for this purpose, manual compensation was introduced to allow volumes to 'interfere'. This allowed distinct scanning strategies to be executed without complication. A commercially available gas atomised Ti-6Al-4V powder feedstock was used in this study. In all builds a, meandering scan strategy was utilised, rotating 67° each successive layer regardless of the layer thickness used.

Table 1. Build parameters for 30μm, 150μm and interlaced specimens for mechanical evaluation including volumetric energy density (VED)

Layer thickness (mm)	Laser Power (W)	Scan speed (mm/s)	VED (J/mm^3)
0.03	100	928.6	42.2
0.15	200	316	70.4

Following removal from the build plate, specimens were turned to meet dimensions. This geometry is stated in ASTM E8M 16a for a reduced size cylindrical test specimen, of 24 mm and 4mm gauge length and diameter respectively. 10 mm diameter grip sections were maintained from the standard – images of final specimens and specimen dimensions are presented in Figure 3. ASTM E8M 16a defines a series of standard specimen geometries for room temperature tensile testing; of which, the reduced size geometry was deemed appropriate for AM samples, to maximise usage of the build envelope as well as material usage. All specimens were observed to fail within the gauge length and as such the method is validated. A standard tensile test system with a crosshead

translation speed of 1 mm/min was used in all tests. Three repeats of each were undertaken.

Optical Images of specimen cross sections were acquired using a Nikon Eclipse LV100ND microscope from specimens which were ground and polished to 1 μm colloidal silica. Grain sizes were evaluated using the ImageJ software. Fracture surfaces were imaged by an Alicona 'Infinite Focus' focus variation microscope (FVM). Point cloud data was then processed using the Mountains 8 surface imaging and metrology software.

3. Results and Discussion

3.1 Layer thickness and joint observations

Typically, LPBF practitioners make use of layer thicknesses which approximate the D_{90} of the powder being used to achieve a layer thickness approximately equal to one powder diameter. As such 30 μm is a common layer thickness used in LPBF. Building dense specimens at 30 μm layers is therefore trivial but depicted in **Figure 2**a for the purpose of comparison. This shows classical grain elongation in the build direction (z) with grains growing across layer interfaces. To successfully build layer thicknesses at 150 μm an increase in volumetric energy density of 66.8% was required. Parameters were based on formative work presented earlier. Here a dramatic change in grain size is observed with elongated grains typically exceeding 1mm in the build direction consistent with [10]. **Figure 2**b shows this effect and individual layers can easily be resolved alongside individual tracks. Lack of fusion pores can also be observed in this field of view which can be attributed to insufficient penetration during keyholing under these conditions. Also evident in the 150 μm micrograph, is a significantly increased fraction of both keyhole and lack of fusion defects.
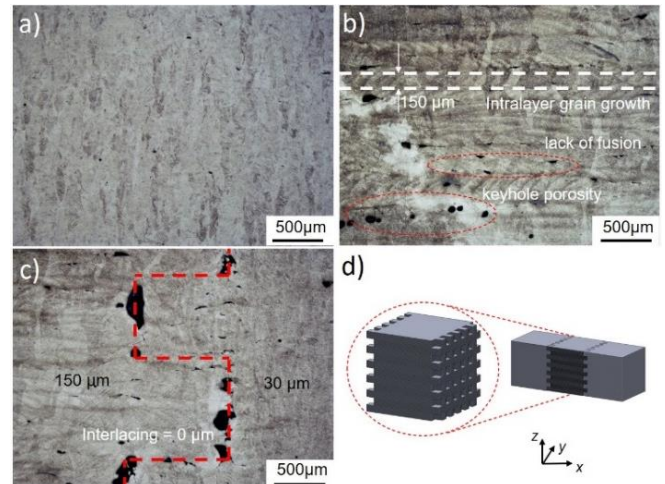
Figure 2. Optical micrographs in the XZ plane: a) 30 μm b) 150 μm c) shows the interface at a castellated union between regions of 150 μm (left) and 30 μm (right). d) shows the schematic joint design

Table 2. Evaluation of grain sizes from Figure 2.

Plane - layer thickness	Avg. grain width (μm)	Avg. grain height (μm)
XZ – 30 μm	102	505
XY – 30 μm	115	92
XZ – 150 μm	291	1052
XY – 150 μm	266	322

The increased energy density necessary to consolidate thicker layers, has also given rise to keyhole pores – formed as recoil pressure from the laser causing molten material to seal over the top of the keyhole cavity. Table 2 highlights the difference in grain size resulting from the difference in layer thickness with a 350% increase in average grain height in the XY plane of the 150 μm compared to the 30 μm specimen.

Figure 2c. shows the interface region formed from interlaced castellated structures which are included here to showcase the design freedoms of this approach. Here regions of differing layer thickness can be united whereby integer multiple layer thickness can be compiled. A more complex component consisting of 30 (grey), 90 (blue) and 150 μm (red) regions can also be conceived (*see* Figure 1. Increasing layer thickness can reduce build time. This typically requires higher energy provision per unit volume. Absolute shrinkage of the consolidated layer becomes more significant at larger layer thicknesses. The lower inset shows a demonstrator arrangement allowing 3-layer thicknesses within a single build.. To achieve this, the 150 and 90 μm regions of the build are subject to laser processing every fifth and third layer, respectively, with no laser processing required for these regions in between these layers.

In **Figure 2**c an interface between 30 μm (right) and 150 μm (left) regions can be seen. The characteristic microstructure of each region is maintained towards the interface at which point large pores can be observed where fusion is poor. This is likely due to an interlacing offset of 0 μm in this case and would be easily overcome by increasing the overlap between regions. **Figure 2**d shows a volumetric representation of the castellated interface. Numerous interface designs may be proposed from this understanding, which allows for optimisation for cycle time particularly where large scan areas are required in large and solid parts.

3.2 Tensile joint behaviour

When compiling individual parts comprised of markedly different regions there is a need to evaluate mechanical performance of the union. Standardized tensile tests were undertaken accordingly.
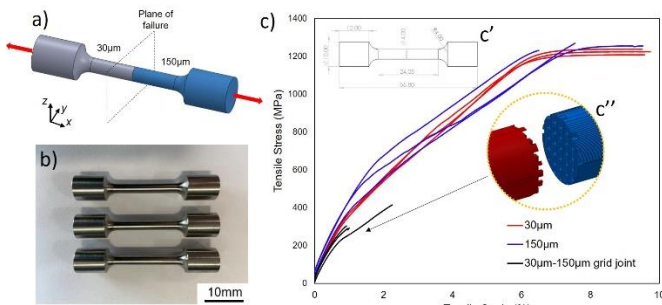
Figure 3. Tensile test results of butt joints and associated grid arrangements give rise to distinct tensile properties and repeatable failure mechanisms. The load direction in all specimens was applied in the 'X' direction parallel to the build plate.

Specimens machined from as-built blanks were stress relieved at 720° for 2 hours and turned to dimension (*see* **Figure 3**b). The specimens comprising regions of 30 and 150 μm layers were arranged such that the union fell at the mid-point of the gauge length, **Figure 3**a. Tensile testing showed similar results in terms of UTS for both 30 and 150 μm specimens with particularly close agreement amongst 30 μm specimens, as could be expected. Spread within the 150 μm specimens is attributed to localised defects which give rise to premature failure, although both series fall within typical SLM (sic) expectations reported in Liu and Shin's review of the mechanical properties of additively manufactured Ti-6Al-4V components (945-1541 MPa) [10]. It should be noted that the range reported in this review includes vertical, horizontal and various heat-treatment strategies. Young's modulus is also more consistent for the 30 μm specimens which is contrasted by the 150 μm which shows greater variation. Liu and Shin's review also underscores the importance of grain texture in mechanical performance associated with additively manufactured components. Given the dominant texture and elongation of grains perpendicular to the loading direction ('X') it is to be expected that

tensile strength and modulus will be distinct for the castellated specimen as compared to the uniform 30 μm equivalent.

The castellated specimens, which unite regions of 150 and 30 μm together, show a dramatically different performance and a 'brittle' failure is observed. Indeed, fracture has occurred ahead of observable plastic deformation. The tensile strength of these specimens is reduced to 25-30% of the 'solid' equivalents. Failure in all three specimens occurred at the interface between the regions.

The apparent tensile performance is easily explained by observation of the micrographs in **Figure 2**. Density of the 30 μm specimen, while not 100%, is notably better than for the 150 μm where lack-of-fusion defects have aggregated interlayer and inter track. These will undoubtedly serve as failure initiation or crack propagation defects. Similarly, the castellated specimens will likely contain lack-of-fusion defects associated with the 150 μm region but failure will be dominated by the lack-of-fusion defects at the interface. The interface of components using this technique will likely always be distinct from the adjacent bulk regions like all fabrications. As such, deployment in component of such structures will require careful consideration of edge effects and their role in defining component integrity. There is also a need to evaluate the loading case in this scenario which cause the castellation side faces to fail under sheer conditions as opposed to tension.

3.3 Fractography

To relate the mechanical response of unions, fractography of specimens was undertaken. Here FVM was used to generate height maps of the fracture surfaces, *see* **Figure 4**.

A characteristic ball (and cup) fracture is observed in **Figure 4** associated with the 30 μm build. Grain scale phenomena are not observable at this magnification and internal defects associated with LPBF processes do not appear to dominate the failure mode. Rather a ductile failure is observed. Two principle plateaus can be observed in this fracture surface (blue-to-yellow) spanning approximately 1 mm. Hence material uniformity and load sharing can be considered superior to the other specimens examined here.
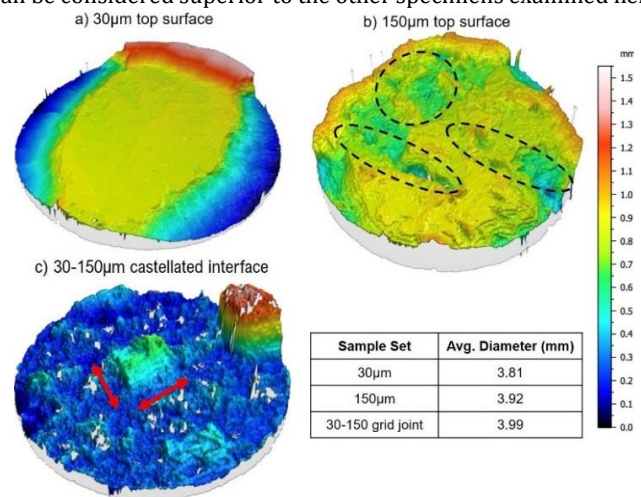
Figure 4. Fractography reveals characteristic failure mechanism associated with build parameters for a) 30, b) 150 and c) 30-150 tensile specimens which also exhibits artefacts approximating the 0.9mm side length castellations. The inset table refers to specimen average diameter following testing.

In contrast failure in the 150 μm specimen (**Figure 4**b) shows a more inconsistent fracture surface comprising both ductile and brittle regions. Failure here can be attributed to the interaction between several distinct defects. From this fracture surface it is possible to observe several regions (enclosed with a broken line) which exhibit rounding at the bottom of the recesses and are likely consistent with lack of fusion/keyhole porosity events. Where

these are in proximity this provides a route for failure and a marked increase in localised stress condition. The surface in this case exhibits a smaller range in heights of 0.6 mm suggesting the failure is accommodated over a narrower band within the specimen and as such there is less opportunity for plastic deformation. This is supported by the coarse measure of necking presented in the table inset to **Figure 4** in which the 30 μm exhibits more constriction, an indication of more plastic deformation.

Figure 4c shows the fracture surface of the castellated specimen. The 'top' surface visible here is from the 150 μm region. It is possible to observe the remnant castellations which are easily identifiable (*see* arrows) as they have maintained their square cross section of 0.9 mm side length. It is of value to note that the mechanism of failure here is not a uniform fracture across the interface rather a more inconsistent fracture which likely relates to differing levels of fusion between the regions. Where castellations are seen to have broken it is proposed that the level of fusion between the 30 and 150 μm regions was superior.

The jagged nature of the fracture surface at the interface, evidenced by increased data drop out (white regions), is also supportive of localised brittle fracture events taking place between lack of fusion pored like those imaged in **Figure 2**c. It is proposed that the level of fusion between layers of distinct thicknesses can be enhanced further by increasing the overlap between parts and thus ensuring a larger fusion region. This may also be used to engineer components with designated failure regions to limit mechanical loads in dynamically loaded structures.

3.4 Multiple interface types and demonstration
To demonstrate the capability of this process the primitive structure shown in **Figure 5** was created. This is composed of 90, 30 and 150 μm layer thickness regions which are interlaced using the same 900 μm castellated approach of the tensile specimens reported earlier.
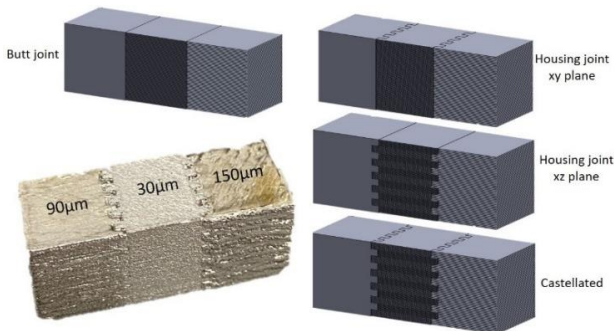
Figure 5. Through adapting the interface design numerous approaches can be proposed which bring together multiple layer thickness arrangements. The photograph illustrates an exemplar component which uses a castellated joint for regions of 90, 30 and 150 μm

The photograph of the demonstrator component comprising 3 regions included in **Figure 5** clearly shows the increase to surface roughness with increasing layer thickness. While this may present challenges for exploitation in the as-built condition, most Ti-6Al-4V components resulting from LPBF will require post process heat treatment and perhaps machining. Thus, presenting limited challenge in some applications. However, surface roughness will be further exaggerated through staircasing in components which do not have a uniform cross section in the build direction. The findings in this study show that a promising methodology for creating components of multiple layer thicknesses can be achieved but the design of the interface between regions of varying layer thicknesses presents a further challenge to optimisation of designs in this space. In their 'hull-bulk' approach de Formanoir et al. effectively used a butt joint arrangement to embed volumes of differing layer thickness size (i.e. 30 and 90 μm only) [3] however,

this is unlikely to provide the optimum union for complex loading arrangements experienced by real components which may experience both torsion and tension. Hence sheer will also play a key role in failure of these interfaces. Through 'in-building' features which interact it is possible to exploit keying mechanisms alongside the fusion achieved through localised welding. As such further exploration of this mechanism is required. It is also proposed that this region does not need to be uniform and could be tapered for example to develop more favourable failure mechanisms such as redirecting cracks in fatigue/creep conditions.

4. Conclusions

A new approach to unite multiple layer thicknesses within a single build to allow an additional design freedom to LPBF practitioners has been presented. An approach can thus be proposed which seeks to strike a balance between increased build rates (through reduced scan times) and maintaining integrity for a particular loading case a component must endure.

- Interlacing of regions within components of different layer thicknesses is perfectly possible and the design of this union can exploit the design freedoms of LPBF techniques.
- This technique can be used to reduce scan times but also modify metallurgy and hence localised properties within a single build. It is feasible that elongation to failure and UTS could easily be tuned within a single component.
- In addition, further properties of structures can be tailored using this approach. Here Ti-6Al-4V is used as the demonstrator material but the principle will apply for any material system processable by LPBF.
- Further experimentation is required to devise appropriate strategies for designing the interlacing approach and functional testing of these in-service conditions.
- To utilise this approach a more advanced assessment method will be required as the basic uniaxial loading schedule employed here is not indicative of freeform component performance.

References
1. D. Bourell, J. P. Kruth, M. Leu, G. Levy, D. Rosen, A. M. Beese, A. Clare, (2017). *Materials for additive manufacturing.* CIRP Annals, **66**(2): p. 659-681.
2. S. Catchpole-Smith, N. Aboulkhair, L. Parry, C. Tuck, I. A. Ashcroft, A. Clare, (2017). *Fractal scan strategies for selective laser melting of 'unweldable' nickel superalloys.* Additive Manufacturing, **15**: p. 113-122.
3. C. de Formanoir, U. Paggi, T. Colebrants, L. Thijs, G. Li, K. Vanmeensel, B. Van Hooreweder, (2020). *Increasing the productivity of laser powder bed fusion: Influence of the hull-bulk strategy on part quality, microstructure and mechanical performance of Ti-6Al-4V.* Additive Manufacturing, **33**: p. 101129.
4. K. A. Sofinowski, S. Raman, X. Wang, B. Gaskey, M. Seita, (2020). *Layer-wise engineering of grain orientation (LEGO) in Laser Powder Bed Fusion of stainless steel 316L.* Additive Manufacturing: p. 101809.
5. J. L. Bartlett, X. Li, (2019). *An overview of residual stresses in metal powder bed fusion.* Additive Manufacturing, **27**: p. 131-149.
6. R. Acharya, J. A. Sharon, A. Staroselsky, (2017). *Prediction of microstructure in laser powder bed fusion process.* Acta Materialia, **124**: p. 360-371.
7. A. T. Clare, W. J. Reynolds, J. W. Murray, N. T. Aboulkhair, M. Simonelli, M. Hardy, D. M. Grant, C. Tuck, (2020). *Laser calorimetry for assessment of melting behaviour in multi-walled carbon nanotube decorated aluminium by laser powder bed fusion.* CIRP Annals, **69**(1): p. 197-200.
8. M. Tang, P. C. Pistorius, J. L. Beuth, (2017). *Prediction of lack-of-fusion porosity for powder bed fusion.* Additive Manufacturing, **14**: p. 39-48.
9. M. J. Matthews, G. Guss, S. A. Khairallah, A. M. Rubenchik, P. J. Depond, W. E. King, (2016). *Denudation of metal powder layers in laser powder bed fusion processes.* Acta Materialia, **114**: p. 33-42.
10. S. Liu, Y. C. Shin, (2019). *Additive manufacturing of Ti6Al4V alloy: A review.* Materials & Design, **164**: p. 107552